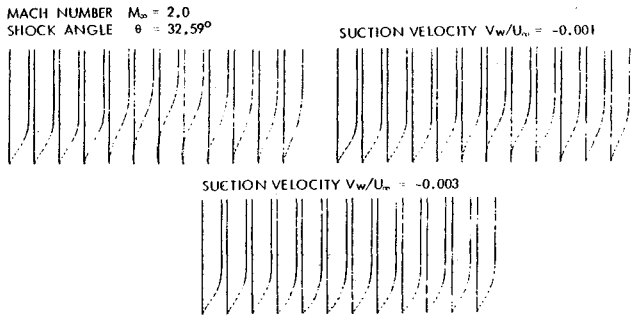

Fig. 4 Velocity profiles in the separated region.

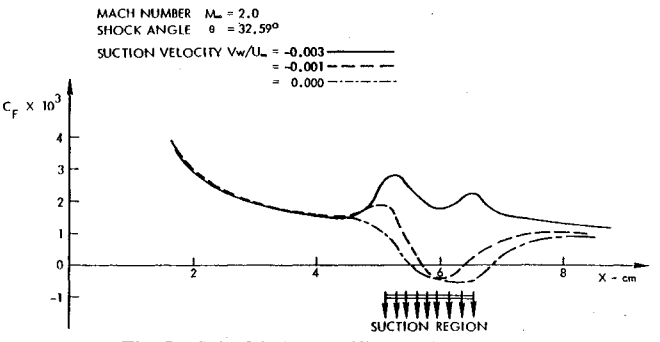

Fig. 5 Skin-friction coefficient distribution.

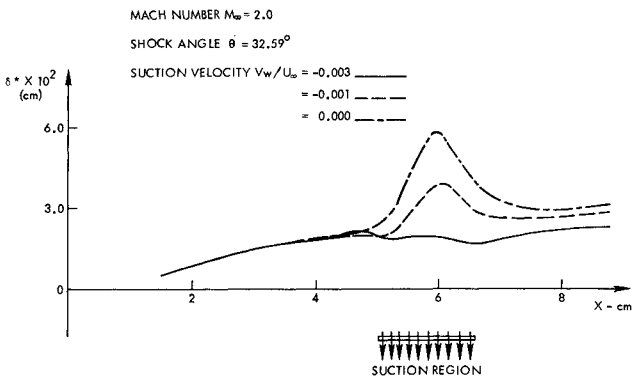

Fig. 6 Displacement thickness distribution.

suction contributes to the stability of the boundary layer. In Fig. 5 the skin-friction coefficient for the three cases are shown for comparison. The wavy nature of the skin-friction coefficient distribution is due to the counteracting effects of the shock adverse pressure gradient and suction. The displacement thickness distribution is plotted in Fig. 6. Even a modest amount of suction of about 0.3% of freestream velocity substantially reduces the boundary-layer thickness in the separation region.

The preceding computations, though preliminary in nature, allow us to predict the effect of suction quantitatively. Currently, investigations are under way to study shock-turbulent boundary-layer suction interaction problems. It is hoped that this work will act as a stepping stone in other important studies of boundary-layer control.

References

[1] Briley, W. R. and McDonald, H., "An Implicit Numerical Method for the Multidimensional Compressible Navier-Stokes Equations," United Aircraft Research Labs., Rept. M911363-6, 1973.

[2] Beam, R. and Warming, R. F., "An Implicit Factored Scheme for the Compressible Navier-Stokes Equations," AIAA Paper 77-645, June 1977.

[3] MacCormack, R. W. and Baldwin, B. S., "A Numerical Method for Solving the Navier-Stokes Equations with Application to Shock-Boundary Layer Interactions," AIAA Paper 75-1, Jan. 1975.

Location and Magnitude of Cascade Shock Loss by High-Speed Smoke Visualization

William B. Roberts*
Nielsen Engineering & Research, Inc., Mountain View, Calif.
and John A. Slovisky†
University of Notre Dame, Notre Dame, Ind.

Introduction

INVESTIGATING the flowfield in a real transonic flow poses several challenges. The use of any type of intrusive probe will not only seriously affect any shock present in the flow but can produce an interfering shock pattern of its own. Also, near a Mach number of one, the flow is extremely sensitive to any area change due to blockage effects. For these reasons, a method that allows quantitative data acquisition without the use of instrusive probes is highly desirable. The high-speed flow visualization technique under development at the University of Notre Dame is such a method, making it possible to determine quantitative data on shock strength and location through a combination of shadowgraph and smoke flow photographs.

The inviscid compressible flow theory predicts a deflection of streamlines passing an oblique or curved shock.[1] The local inclination of the shock to the upstream direction, together with the deflection of the streamline through the shock, can be used to determine the upstream and downstream Mach numbers across the shock. The pertinent relationships from the compressible flow theory are:

$$\tan\theta = 2\cot\psi\left[\frac{M_1^2\sin^2\psi - 1}{M_1^2(k+\cos 2\psi)+2}\right] \tag{1}$$

$$M_2^2\sin^2(\psi-\theta) = \frac{1+\left(\frac{k-1}{2}\right)M_1^2\sin^2\psi}{kM_1^2\sin^2\psi - \left(\frac{k-1}{2}\right)} \tag{2}$$

where: M_1 and M_2 = upstream and downstream Mach number respectively; ψ = local inclination angle of shock with upstream flow; θ = streamline deflection through shock wave; and k = ratio of specific heat. They are illustrated in Fig. 1. If the local shock inclination ψ, together with the deflection θ, along streamlines could be determined along a shock wave, then the upstream and downstream Mach numbers could be calculated and the shock pressure ratio and loss determined.

Test Equipment and Procedure

All testing was done in the Planar High-Speed Smoke Tunnel (PHSST) at the Aerospace Laboratory of the University of Notre Dame. A complete description and drawings of the PHSST are given in Refs. 2 and 3. The

Presented as Paper 79-0042 at the AIAA 17th Aerospace Sciences Meeting, New Orleans, La., Jan. 15-17, 1979; submitted Jan. 31, 1979; revision received June 22, 1979.

Index categories: Transonic Flow; Nozzle and Channel Flow; Airbreathing Propulsion.

*Project Engineer. Member AIAA.
†Research Assistant, Dept. of Aerospace and Mechanical Engineering. Member AIAA.

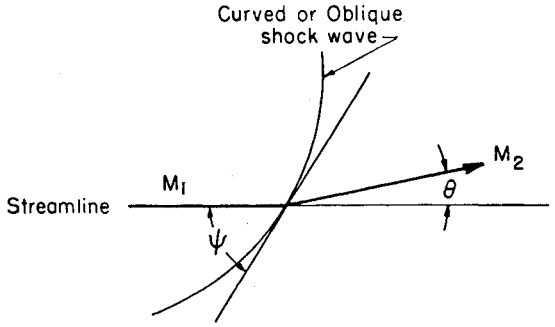

$$\text{Tan}\,\theta = 2\cot\psi\left[\frac{M_1^2\sin^2\psi - 1}{M_1^2(k+\cos 2\psi)+2}\right] \qquad (1)$$

$$M_2^2\sin^2(\psi-\theta) = \frac{1+\left(\frac{k-1}{2}\right)M_1^2\sin^2\psi}{kM_1^2\sin^2\psi - \left(\frac{k-1}{2}\right)} \qquad (2)$$

Where: M_1 – Upstream Mach No.

M_2 – Downstream Mach No.

ψ — Local inclination angle of shock with upstream flow

θ — Streamline deflection through shock wave

k — Ratio of specific heat

Fig. 1 Relations between shock inclination, deflection, and upstream and downstream Mach number.

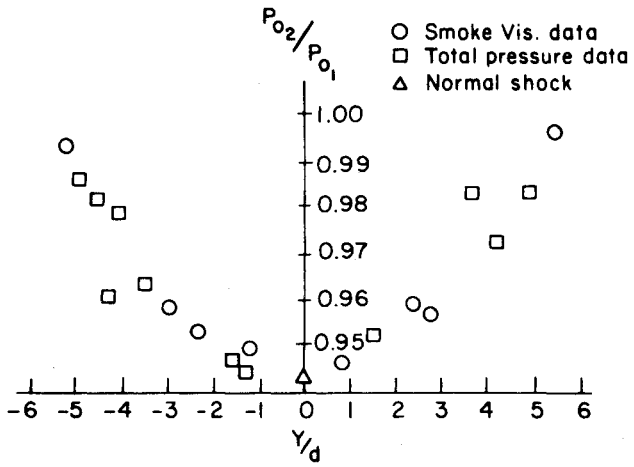

Fig. 2 Nondimensional distance along shock vs total pressure ratio for cylinder, $M_\infty = 1.45$, $Re = 50{,}000$.

PHSST is of the air indraft type and consists of inlet screens, contraction nozzle, test section, and diffuser. It is capable of being connected to one, two, or three 1.47 m^3/s vacuum compressors. The inlet screens consist of seven no. 20 mesh wire screens before the contraction nozzle to reduce the turbulence of the flow. The present tunnel has an area ratio of 92.5:1 between the inlet and the throat. The test section is 4.1×10.8 cm (44.2 cm^2) with an area ratio of 1.26 between it and the throat. This constant area section is approximately 7.62 cm long.

Smoke particles of ~ 0.7 μm are generated by dripping kerosene onto electric strip heaters.[4] It is then forced by a blower through a laterally adjustable smoke rake which cools the smoke to room temperature. When the rake is placed flush with the first screen at the tunnel inlet, the smoke is drawn into the contraction nozzle and through the test section in continuous filaments or lines. The integrity of these

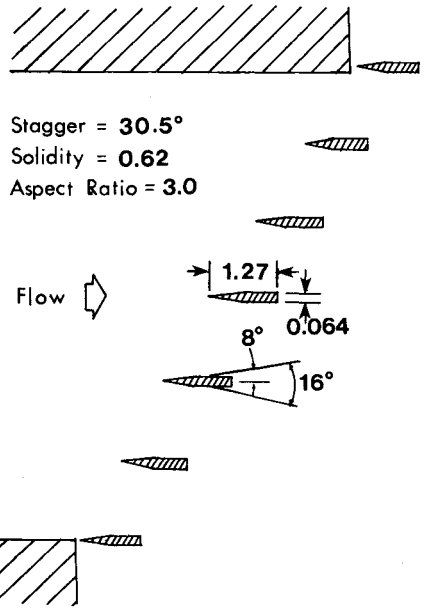

Fig. 3 Preliminary high-speed smoke visualization cascade (dimensions in cm).

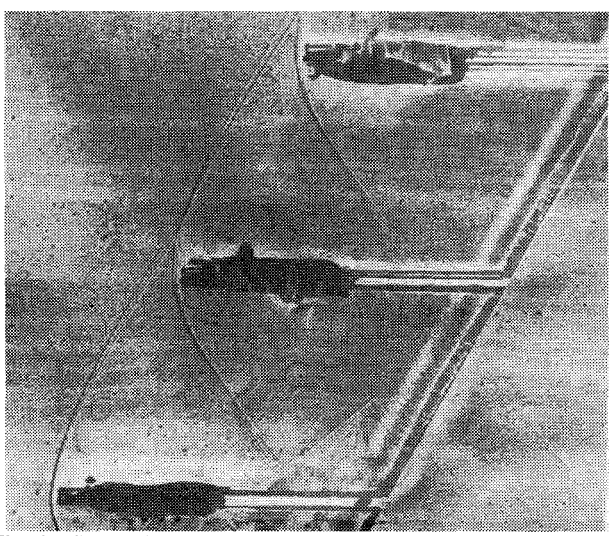

Fig. 4 Composite photograph of PHSSVC in PHSST at $M_1 = 1.29$, incidence = 1.75 deg.

smokelines is maintained because of the low turbulence brought about by the screening and contraction nozzle. Since the smoke is ingested at stagnation temperature, it shows no buoyancy effects as it passes through the test section. A seed particle trajectory analysis given in Ref. 5 indicates that, within the length of a shock wave after passing through a shock, a seed particle will follow the flow within 1-2% of the velocity and 1 deg of direction.

Total pressure readings were taken using a three-pronged pitot-tube rake capable of vertically traversing three-fourths of the test section height and a single-prong pitot probe capable of vertically traversing the entire test section.

Smoke pictures were taken with a Graphlex Graphite View 4×5 camera with an Ilex No. 3 Acme Syncro Shutter lens using Kodak Royal Pan-X film (ASA film speed 1250). The smoke was illuminated by four Strobolume high-intensity strobes, two firing through the transparent top and two through the bottom walls of the test section. Shadowgraphs were produced by exposing 8×10 sheets of Kodak Royal Pan film to a point source of light passing through the test section. All film was developed in Kodak D-11 for 13 min; printing and enlarging was done on a Federal 4×5 enlarger using

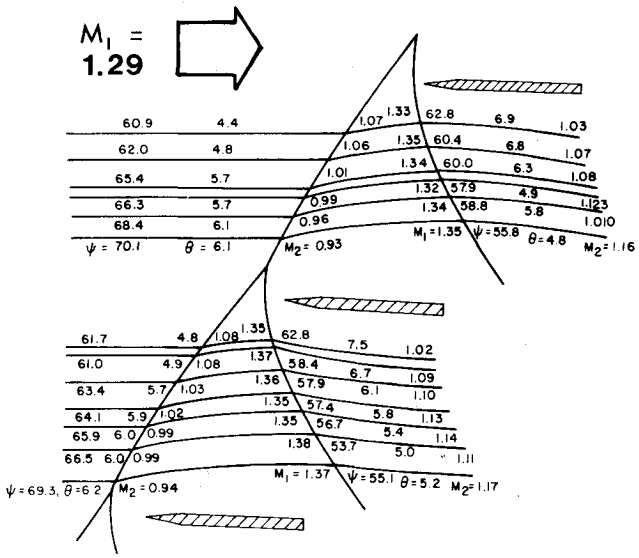

Fig. 5 Flowfield determination of PHSSVC in PHSST at $M_1 = 1.29$, incidence = 1.75 deg.

Kodabromide F5 high-contrast photographic paper in a developer solution of two parts water to one part Dektol.

A standard test proceeded as follows: After the tunnel was started, the total pressure rake was moved to a predetermined location. Total pressure readings were then taken off a mercury manometer board (within ±2.5 mm Hg accuracy) and a shadowgraph was taken. The smoke generator was then started and smoke entered the test section. Smoke photo exposure times varied from 1/10th to 1/50th s at aperture settings from *f*4.5 to *f*8.0. After this, the pitot rake was moved to another position and the procedure repeated until all appropriate probe positions were examined. The smoke and shadowgraph negatives for each probe position were both enlarged to the same scale and superimposed on each other. This procedure assumes steady flow and has produced good results. From these enlargements, the shock inclination and streamline deflections were measured optically and graphically to within ± 1 deg.

Although the major goal of this testing program is to prove the applicability of this technique to cascades, it was felt the concept should be proven first using simpler geometries. Therefore, a number of two-dimensional shapes were tested, such as a cylinder, various wedge and flat-top airfoils, and a Whitcomb supercritical wing section. These tests indicated that the method was reliable for oblique and curved shocks. An example is shown in Fig. 2, which is a comparison of total pressure ratio across the curved bow shock of a circular cylinder measured by a total pressure probe and the smoke visualization technique. As can be seen, the data correlate well. Further results are given in Ref. 2.

The cascade test configuration was the Preliminary High-Speed Smoke Visualization Cascade (PHSSVC) and is seen in silhouette in Fig. 3. It consisted of seven flat plates with a leading-edge, double-wedge angle of 16 deg. The chord length is 1.27 cm with a thickness-to-chord ratio of 5%, stagger angle of 30.5 deg, solidity of 0.62, and aspect ratio of 3.0.

Results

Figure 4 is a composite photograph of transonic flow in the PHSSVC. In it the smokelines can be seen being deflected upward through the front shock, curving as the gas is re-expanded up to the passage shock where the smokelines are deflected downward to the near-axial direction. A series of oblique shocks emanating from the blunt trailing edges of the blades can also be seen. However, these will be extremely weak, as indicated by their low wave angles and small deflections, and were not studied. From a series of photographs, such as Fig. 4, the flowfield determination of Fig. 5 was made. From this, the inlet shock total pressure ratio can be isolated and the shock loss coefficient calculated. More detailed results are presented in Ref. 2.

Conclusions

This combined visualization technique should prove useful in examining the flow through the leading-edge regions of transonic cascades and make it possible to isolate the shock loss from the end-wall and profile losses.

Acknowledgment

This work was sponsored in part by the Fan and Compressor Branch of the NASA/Lewis Research Center, under Grant MSG-3133.

References

[1] Shapiro, A. H., *The Dynamics and Thermodynamics of Compressible Fluid Flow*, Vol. 1, Roland Press Company, New York, 1953, p. 529.

[2] Slovisky, J. A., Roberts, W. B., and Crouse, J. A., "High Speed Smoke Visualization for the Determination of Cascade Shock Losses," AIAA Paper 79-0042, New Orleans, La., Jan. 1979.

[3] Goddard, V. P., McLaughlin, J. A., and Brown, F. N. M., "Visual Supersonic Flow Patterns by Means of Smoke Lines," *Journal of the Aerospace Sciences*, Vol. 26, Nov. 1959, pp. 761-762.

[4] Holman, J. P., *Experimental Methods for Engineers*, McGraw-Hill Book Co., Inc., New York, 1978, p. 438.

[5] Wisler, D. C., "Shock Wave and Flow Velocity Measurements in a High Speed Fan Rotor Using the Laser Velocimeter," ASME Paper 76-GT-49, March 1976.

Thermal Analysis of a Conical Cathode of an MPD Arc

R. C. Mehta*
Vikram Sarabhai Space Centre, Trivandrum, India

Nomenclature

Bi = Biot number = hL/k, nondimensional
h = heat-transfer coefficient
I = applied current
j = current density
k = thermal conductivity
L = cathode length
Q_s = heat transfer to cathode root
Q_0 = heat transfer to cathode coolant water
r = cathode radius
r_0 = cathode tip radius
T = local temperature of cathode at x
T_s = cathode temperature at $X = 0$
T_0 = cooling water temperature at $X = 1$
T_∞ = surrounding temperature
x = space coordinate
X = nondimensional length, x/L
X_1 = nondimensional conical length of cathode, L_1/L
α = semicone angle
ϵ = emissivity
θ = nondimensional temperature, T/T_s
ρ = electrical resistivity
σ = Stefan-Boltzmann constant

Received Feb. 15, 1979; revision received May 8, 1979.

Index categories: Electric and Advanced Space Propulsion; Plasma Dynamics and MHD; Radiation and Radiative Heat Transfer.

*Engineer, Propulsion Engineering Division (PSN).